Ferromagnetic insulating phase in $Pr_{1-x}Ca_xMnO_3$

R. Kajimoto*
Department of Physics, Ochanomizu University, Bunkyo-ku, Tokyo 112-8610, Japan

H. Mochizuki and H. Yoshizawa
Neutron Science Laboratory, Institute for Solid State Physics, University of Tokyo, Tokai, Ibaraki 319-1106, Japan

S. Okamoto†
Institute of Physical and Chemical Research (RIKEN), Saitama 351-0198, Japan

S. Ishihara
Department of Physics, Tohoku University, Sendai 980-8578, Japan

(Received 24 June 2003; revised manuscript received 29 October 2003; published 27 February 2004)

A ferromagnetic insulating (FM-I) state in $Pr_{0.75}Ca_{0.25}MnO_3$ has been studied by neutron scattering experiment and theoretical calculation. The insulating behavior is robust against an external magnetic field, and is ascribed to neither the phase separation between a ferromagnetic metallic (FM-M) phase and a nonferromagnetic insulating one, nor the charge ordering. We found that the Jahn-Teller type lattice distortion is much weaker than $PrMnO_3$ and the magnetic interaction is almost isotropic. These features resemble the ferromagnetic metallic state of manganites, but the spin exchange interaction J is much reduced compared to the FM-M state. The theoretical calculation based on the staggered type orbital order well reproduces several features of the spin and orbital state in the FM-I phase.

DOI: 10.1103/PhysRevB.69.054433 PACS number(s): 75.47.Lx, 75.47.Gk, 75.25.+z, 75.30.Ds

I. INTRODUCTION

Since the discovery of the high-T_c superconductivity in layered cupurates, doped Mott insulators with perovskite structures became one of the major targets in recent studies of condensed matter physics. Hole doped perovskite manganites, $R_{1-x}A_xMnO_3$ (R is a trivalent rare-earth ion and A is a divalent alkaline-earth ion), have been extensively studied since the discovery of the colossal magnetoresistance (CMR) effect. Recent studies devoted to clarify an origin of the CMR effect have revealed that the physics of manganites is controlled by an interplay between spin, charge and orbital degrees of freedom.

At $x=0$ in $R_{1-x}A_xMnO_3$, a Mn ion shows an electron configuration of $t_{2g}^3e_g^1$ where the e_g orbital degree of freedom is active. Actually, the mother compound $RMnO_3$ shows an alternate ordering of the $d_{3x^2-r^2}$ and $d_{3y^2-r^2}$ orbitals associated with the cooperative Jahn-Teller distortion in the *ab* plane of the orthorhombic *Pbnm* lattice. The layer-type (A-type) antiferromagnetic (AF) spin ordering is realized at low temperature by the anisotropic superexchange interaction under the orbital ordering (OO).[1–3] This anisotropy was experimentally confirmed in $LaMnO_3$ by neutron scattering studies.[4,5] By substituting R for A in $RMnO_3$, holes are introduced in the system. In the simple double exchange scenario, a kinetic energy gain of the doped holes brings about the ferromagnetic metallic (FM-M) ground state.[3,6] It is also supposed that the OO is destroyed and the orbital liquid/disordered states are realized in the FM-M phase.[7] The isotropic characters in the crystal lattice[8] and the spin exchange interactions[9,10] realized in this phase may be attributed to this orbital state.

However, in the actual compounds, the doping dependence of the electronic ground state is not so naïve. Between the A-type AF phase and the FM-M phase, the ground state is ferromagnetic but insulating.[3] The ferromagnetic insulating (FM-I) state cannot be explained by the simple double exchange picture. Although such a contradiction remains to be solved, the FM-I phase has not been much studied so far. This paper provides detailed information about the character of the FM-I phase by a neutron scattering study and a theoretical calculation on $Pr_{1-x}Ca_xMnO_3$, which is a typical example of a FM-I phase with a relatively wide hole concentration region $0.15<x<0.3$.[11]

One of the interpretations of the FM-I phase is based on a phase separation between the FM-M phase and a non-FM insulating phase. In a recent trend of the research on CMR manganites, the phase separation phenomenon is regarded as an important factor for the large resistivity change accompanied by the insulator-metal (IM) transition. A plausible origin of the non-FM insulating phase is the *CE*-type charge ordering (CO). This is a checkerboard-type CO of Mn^{3+} and Mn^{4+} accompanied by a zigzag ordering of $d_{3x^2-r^2}$ and $d_{3y^2-r^2}$ orbitals on Mn^{3+} sites and the *CE*-type AF spin ordering. The *CE*-type CO is most stabilized at $x=1/2$, but it is exceedingly robust against hole doping. Actually, in $Pr_{1-x}Ca_xMnO_3$, the *CE*-type CO is well developed for $x \geqslant 0.3$ adjacent to the FM-I phase, and coexists with the FM component.[11–13] Recently, Dai *et al.* showed by neutron scattering measurement that the short-range order of the *CE*-type CO exists in the FM-I phase of $La_{1-x}Ca_xMnO_3$,[14] though the detail relation between these charge correlations and the transport is not obvious.

The phase separation picture requires substantial volume fraction of non-FM insulating phase to make the compound an insulator overcoming the metallic conduction in the FM

phase. Uehara *et al.* studied the phase separation between the FM-M phase and the charge-ordered insulating (CO-I) phase in $La_{5/8-y}Pr_yCa_{3/8}MnO_3$. They showed that the concentration of the FM-M phase at the IM transition, which was evaluated from the ratio of the saturation magnetic moment to the full moment of a Mn ion, agrees with the three-dimensional (3D) percolation threshold 10–25%.[15] However, the FM moment of $\sim 2\mu_B$ in $Pr_{0.7}Ca_{0.3}MnO_3$[12,13,16] is too large to account for its insulating character. On the other hand, there is another possibility that the insulating nature does not arise from the non-FM phase but it is intrinsic to the FM phase. Recently several kinds of COs related to the hole concentration of $x=1/4$ were theoretically proposed. Hotta *et al.* claimed that $Pr_{3/4}Ca_{1/4}MnO_3$ becomes a FM-I state by a CO consisting of a checkerboard charge ordered plane and a purely Mn^{3+} plane stacking alternately along the z axis.[17] As a result, the unit cell of the CO becomes $\sqrt{2}\times\sqrt{2}\times 4$ in terms of the cubic perovskite unit [We will refer this type of CO as $(\pi,\pi,\pi/2)$-type CO.]. Mizokawa *et al.* proposed that in the lightly doped manganites there exist ''orbital polarons.'' Here Mn^{4+} ions are surrounded by ferromagnetically coupled nearest neighbor Mn^{3+} ions where the e_g orbitals point to the central Mn^{4+} site.[18] They claimed that in $Pr_{3/4}Ca_{1/4}MnO_3$, the orbital polarons form a body-centered-cubic lattice whose unit cell has a size of $2\times 2\times 2$ in unit of the cubic perovskite lattice, and a FM insulator is realized.[19] Neither kind of CO, however, has not been detected experimentally so far. Instead, Endoh *et al.* claimed by resonant x-ray scattering (RXS) and neutron scattering studies that the FM-I phase of $La_{0.88}Sr_{0.12}MnO_3$ shows an OO of a mixture of $d_{3z^2-r^2}$ and $d_{x^2-y^2}$ orbitals. They also proposed that this OO is an origin of the FM-I state.[20,21] As for the orbital state of the FM-I phase in $Pr_{1-x}Ca_xMnO_3$, Zimmermann *et al.* advocated by a RXS study that the same OO as that in $LaMnO_3$ ($LaMnO_3$-type OO) develops below about 500 K in $Pr_{0.75}Ca_{0.25}MnO_3$.[22] In contrast to the FM spin ordering in $Pr_{0.75}Ca_{0.25}MnO_3$, however, $LaMnO_3$-type OO is generally accompanied with an *A*-type AF spin ordering.

The complicated status of the current research on the FM-I state of manganites reminds us the necessity of a comprehensive study on spin, charge, and orbital states of the FM-I phase of manganites. For this purpose, neutron scattering is a useful tool to study CO and OO because of its sensitivity to the lattice distortions induced by CO and OO. In the present study, we performed elastic neutron scattering measurements on a single crystal of $Pr_{0.75}Ca_{0.25}MnO_3$ to elucidate the superlattice peaks and the lattice distortions due to CO and OO. The OO affects the exchange interactions between spins due to the anisotropic character of the e_g orbitals. Therefore, through the estimation of the exchange interactions by measuring the magnon dispersion relation, we can characterize the orbital state. So, we also performed inelastic neutron scattering measurements to determine the spin exchange through the measurements of the spin wave excitations. The theoretical analyses provide a unified picture for the spin and orbital states in the AF, FM-I and FM-M phases.

The rest of this paper is organized as follows. In Sec. II, the experimental procedure is described. The experimental results are presented in Sec. III, where the property of the magnetic and crystal structures in $Pr_{0.75}Ca_{0.25}MnO_3$ are discussed. In Sec. III A, we will argue the possibility of the phase separation, and in Sec. III B we will characterize the FM-I state by measurements of the structural properties and spin fluctuations. Section III C is devoted to a theoretical investigation of the magnetic interaction and the orbital state in moderately doped manganites. A summary of the work is given in Sec. V.

II. EXPERIMENTAL PROCEDURES

Single crystals of $Pr_{0.75}Ca_{0.25}MnO_3$ and $PrMnO_3$ were grown by the floating zone method. A stoichiometric mixture of Pr_6O_{11}, $CaCO_3$, and Mn_3O_4 was ground and calcined at 1300 °C in air for 12 h. Then the resulting powder was pressed into rods and fired again at 1300 °C in air for 12 h. The crystal growth was performed in a floating-zone furnace in a flow of oxygen gas. We precharacterized the samples by powder x-ray diffraction and powder neutron diffraction measurements, and confirmed that the samples are single phase with the *Pbnm* symmetry. The lattice constants of $Pr_{0.75}Ca_{0.25}MnO_3$ at 294 K determined by the powder neutron diffraction are $a=5.4444(3)$ Å, $b=5.5037(3)$ Å, and $c=7.6880(5)$ Å. The samples were cut into the size of 6 mm$\phi\times$30 mm for the present neutron scattering study. The transport data were taken using Quantum Design Physical Property Measurement System (PPMS) on a sample cut from the same batch as used in the neutron study.

The neutron scattering experiments were performed using triple axis spectrometers GPTAS and HQR of Institute for Solid State Physics, University of Tokyo, installed at the JRR-3M research reactor in JAERI, Tokai, Japan. The most of the measurements were done at GPTAS, while HQR was utilized when a high Q resolution was required. At both spectrometers, the 002 reflection of pyrolytic graphite (PG) was used for the monochromator and analyzer. At GPTAS, we selected a neutron wave length of $k_f=3.81$ Å^{-1}. For elastic scattering measurements, several combinations of horizontal collimators were adopted and two PG filters were placed before the monochromator and after the sample to suppress contaminations of higher-order harmonics. For inelastic scattering measurements, we chose 40′-40′-40′-40′ combination of collimators and set a PG filter after the sample. At HQR, which is on the thermal guide tube, neutrons of wave length $k_i=2.56$ Å^{-1} and horizontal collimation of blank-40′-40′ (from monochromator to sample) were used together with a PG filter before the sample. The crystals were mounted in aluminum cans filled with helium gas. The temperature of the samples were controlled by conventional and high-temperature-type closed cycle He-gas refrigerators. The measurements were performed in the $(h,0,l)$ and (h,h,l) zones of reciprocal space of the *Pbnm* lattice.

III. RESULTS AND DISCUSSIONS

A. Possibility of the phase separation

First, let us characterize the sample by showing the results of the temperature (T) dependences of the order parameter of the magnetic order and the resistance. Figure 1(a) is the T

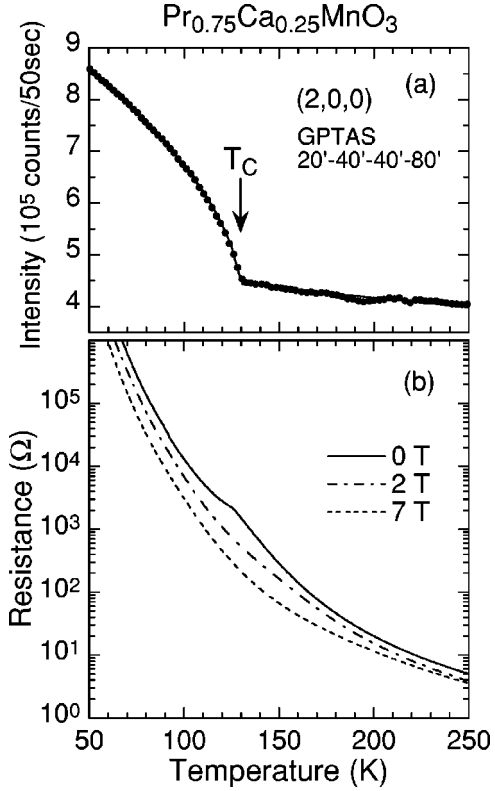

FIG. 1. (a) Temperature dependence of the scattering intensity of the 200 peak. (b) Temperature dependence of the resistance under the magnetic field of $H=0$, 2, and 7 T.

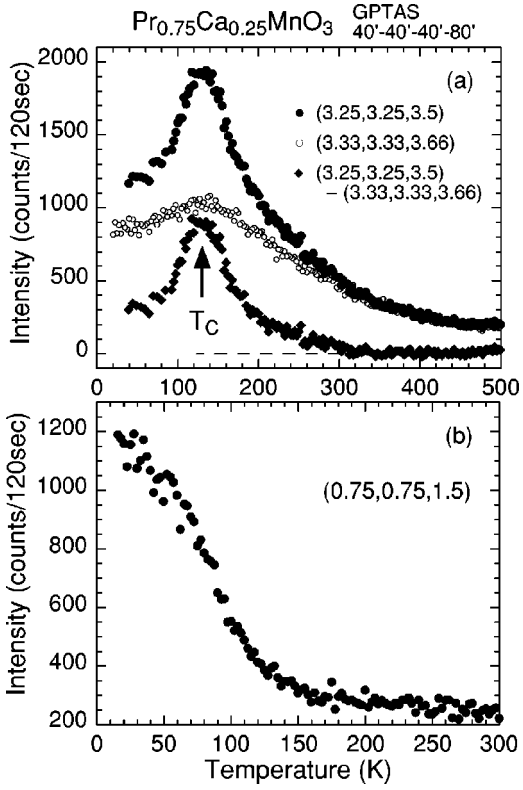

FIG. 2. (a) T dependence of the intensity of the *CE*-type charge/orbital order peak at $\boldsymbol{Q}=(3.25,3.25,3.5)$. Closed circles: the raw scattering intensity at (3.25,3.25,3.5). Open circles: the intensity due to the Huang scattering measured at (3.33,3.33,3.66). The intensity of 100 counts is subtracted to compensate for the difference in background intensity at the two positions. Diamonds: net intensity due to the *CE*-type CO. (b) T dependence of the intensity of the pseudo-*CE*-type AF peak at $\boldsymbol{Q}=(0.75,0.75,1.5)$.

dependence of the scattering intensity of the fundamental 200 peak. The intensity starts to increase below the Curie temperature $T_C\sim 130$ K due to the FM spin ordering, consistent with a previous study.[11] To determine the critical exponent, we fit the data to a power law, $(1-T/T_C)^{2\beta}$, varying the lower limit of the temperature range of the fitting, $T_{\rm lim}$. β was determined to be 0.36(1) as $T_{\rm lim}\rightarrow T_C=129.5(5)$ K. This value of the critical exponent is very close to that for the 3D FM Heisenberg model, 0.367, and similar to that for the FM-M manganites such as $La_{0.7}Sr_{0.2}MnO_3$ (Ref. 23) and $La_{0.7}Sr_{0.3}MnO_3$.[9,23] The magnetic moment was determined from a powder sample which was prepared by crushing a melt-grown crystal. The FM moment of a Mn ion is $3.32(3)\mu_B$ at 15 K, oriented parallel to the b axis. The magnetic moments of Pr ions also align ferromagnetically along the b axis with a moment of $0.55(3)\mu_B$/Pr at 15 K, consistent to $x=0.2$ and 0.3 samples.[16,24] The value of the FM moment of a Mn ion is nearly equal to the formula value of $3.75\mu_B$. This means that even if a non-FM region existed in the sample, its volume would be extremely small.

Figure 1(b) shows the T dependence of the resistance at several magnetic fields. For $H=0$ T, the sample is insulating for all temperature range measured, and a small cusp is observed at T_C. By applying the magnetic field, this cusp vanishes, and the resistance is reduced from that at $H=0$ T. However, the insulating behavior still persists under the magnetic field up to $H=7$ T. The robustness of the insulating state contrasts markedly with the *CE*-type charge ordered phase for $x>0.3$, where the CO melts by a magnetic field of a few teslas.[11] In the present case, an external field cannot make a significant change of the transports. Note that similar behaviors have been observed in a less doped FM sample $x=0.2$.[24]

The above-mentioned magnetic and transport properties indicate that the origin of the insulating behavior of $Pr_{0.75}Ca_{0.25}MnO_3$ is definitely different from the *CE*-type CO, and suggests that it is intrinsic to the FM state. To confirm this point, we performed the neutron diffraction measurements and surveyed reciprocal points to detect signals due to the *CE*-type CO, and found the lattice superlattice peaks due to the *CE*-type CO. Figure 2 shows a T dependence of the scattering intensity at $\boldsymbol{Q}=(3.25,3.25,3.5)$ (closed circles), which corresponds to a *CE*-type CO peak (5,1.5,0) (Ref. 25) of a different domain of the sample. Because diffuse scattering due to single polarons (Huang scattering) overlaps at this position,[27] the intensity of the diffuse scattering estimated at $\boldsymbol{Q}=(3.33,3.33,3.66)$ (open circles) is subtracted from the data to obtain the net scattering intensity due to the *CE*-type CO (diamonds). The *CE*-type CO develops below $T\sim 320$ K. It is drastically suppressed below T_C, although the sample remains insulating [Fig. 1(b)]. The small cusp of the resistance at T_C may be related to the melting of the *CE*-type CO, but the overall insulating feature of the

resistance, however, cannot be explained by the *CE*-type CO. This is in contrast to the FM-M region of manganites, where the disappearance of the short-range *CE*-type CO accompanies the transition to the FM-M state.[14,27,28] We also found the pseudo *CE*-type AF peaks concomitant with the *CE*-type CO in the region of $x<1/2$ [Fig. 2(b)].[12,13,16,29] Their intensity is of the order of 10^{-3} in comparison with that of the FM peak [Fig. 1(a)], indicating that the volume of the *CE*-type CO phase is negligible.

B. Character of the FM-I state

The results described in Sec. II A indicate the phase separation between the FM-M phase and the non-FM insulating phase is not important for the FM-I phase of $Pr_{1-x}Ca_xMnO_3$. The FM-I state is an intrinsic state of the low doped region of manganites. Consequently, to understand the FM-I phase, we will characterize the charge and orbital states in this phase.

First, we tried to clarify whether the FM-I state is a FM charge ordered state as theoretically proposed. For the $(\pi,\pi,\pi/2)$-type CO proposed by Hotta *et al.*,[17] the superlattice peaks are expected at $\boldsymbol{Q}=(h,k,l)$ with $h+k=$odd and $l=$half integer. To detect this type of CO, we surveyed $(m,0,1/2)$ and $(5,0,n/2)$ positions where m and n are odd integers, but could not find any peaks [Fig. 3(a)]. This result is negative for the existence of this type of charge order in $Pr_{0.75}Ca_{0.25}MnO_3$.

The orbital polaron lattice proposed by Mizokawa *et al.*[18,19] will produce superlattice reflections at $\boldsymbol{Q}=(h,k,l)$ with ($h+k=$odd and $l=$even) or ($h,k=$half integer and $l=$odd). We found peaks at several positions satisfying these conditions and forbidden by the *Pbnm* symmetry [Fig. 3(b)]. Unfortunately, however, these positions coincide with those with integer indices considering the twinning of the crystal [for Fig. 3(b), (1.5,1.5,3) and (2.5,2.5,5) correspond to (3,0,0) and (5,0,0) of a different domain, respectively.], and additional small tilts of MnO_6 octahedra can produce Bragg peaks at such positions. We mention that these peak intensities do not show a common temperature dependence following that in the resistivity [for example, in Fig. 3(b), the intensity at 300 K is strongest for the (2.5,2.5,5) peak while the 500 K data are strongest for the (1.5,1.5,3) peak]. Therefore, we speculate that these peaks are attributed to the Bragg reflections from the alternate domain in the twinning crystal, although further experiments are required to conclude this.

Next, we will investigate the orbital state of the FM-I state. According to the recent RXS study, resonant signals observed in $Pr_{0.75}Ca_{0.25}MnO_3$ are consistent with the same OO as $LaMnO_3$, i.e., an alternate ordering of $d_{3x^2-r^2}$ and $d_{3y^2-r^2}$ orbitals in the *ab* plane.[22] $LaMnO_3$-type OO is expected to produce significant anisotropies in the crystal structure as well as spin exchange: The in-plane lattice constants *a* and *b* become longer than the out-of-plane lattice constant *c*, and the exchange interactions within the *ab* plane will be stronger than that along the *c* axis. Therefore, measuring these quantities should be useful for quantitative understanding of the orbital state.

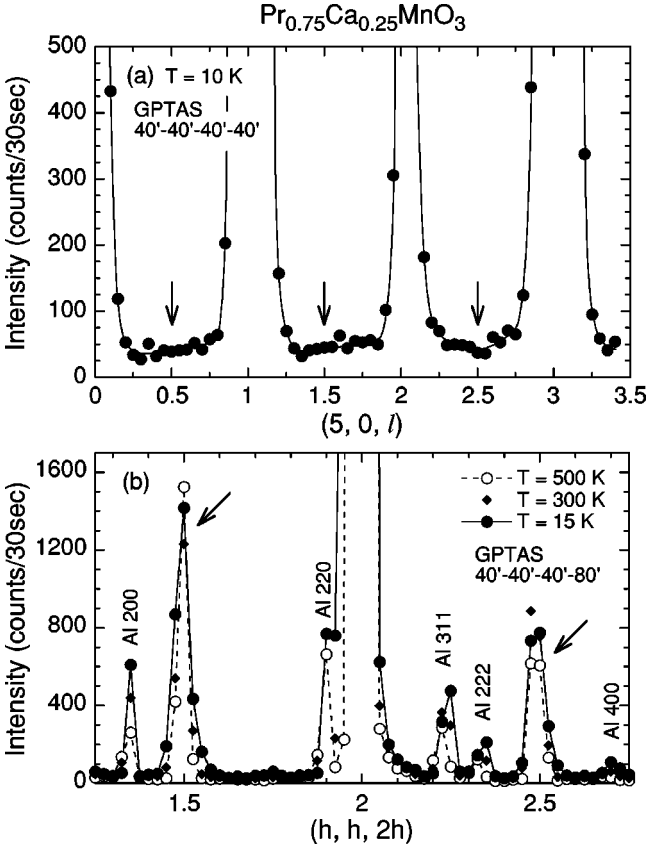

FIG. 3. (a) Profiles along the (5,0,l) line at 10 K. Arrows indicate positions where superlattice peaks due to the $(\pi,\pi,\pi/2)$-type CO are expected. (b) Profiles along the ($h,h,2h$) line at 500, 300, and 15 K. Arrows indicate positions where superlattice peaks due to the orbital polaron lattice are expected. "Al" labels diffraction peaks from the aluminum sample cell. Lines are guides to the eyes.

Figure 4(a) shows neutron diffraction profiles of $Pr_{0.75}Ca_{0.25}MnO_3$ around the fundamental (2,2,0) position along the [110] direction at 100 and 560 K. Because of the twinning, the 004 peak is also observed at slightly higher Q than the 220 peak. At $T=560$ K, both peaks locate so close that the observed profile forms almost a single peak. On the other hand, this peak splits into two peaks at $T=100$ K due to the small increase of the *a* or *b* axis and the large decrease of the *c* axis. This change of the lattice constants is consistent with the cooperative Jahn-Teller distortions accompanied by the $LaMnO_3$-type OO. We measured T dependences of similar profiles and found that the structural change gradually develops below $\sim$450 K. This temperature coincides with the temperature where the orbital signals measured by the RXS study starts to increase,[22] and corresponds to the transition temperature from the *O* phase to the *O'* phase identified in Ref. 29. These results qualitatively suggest the developing of the $LaMnO_3$-type OO below $T\sim450$ K. However, the amplitude of the lattice distortion is fairly small compared to the mother compound, $PrMnO_3$, where a typical $LaMnO_3$-type OO is expected. This can easily be assured by comparing the profile of the 220/004 reflections for both compounds. In Fig. 4(b), we depicted the profiles of the 220 and 004 reflections of $PrMnO_3$ at $T=8$ K. The Jahn-Teller

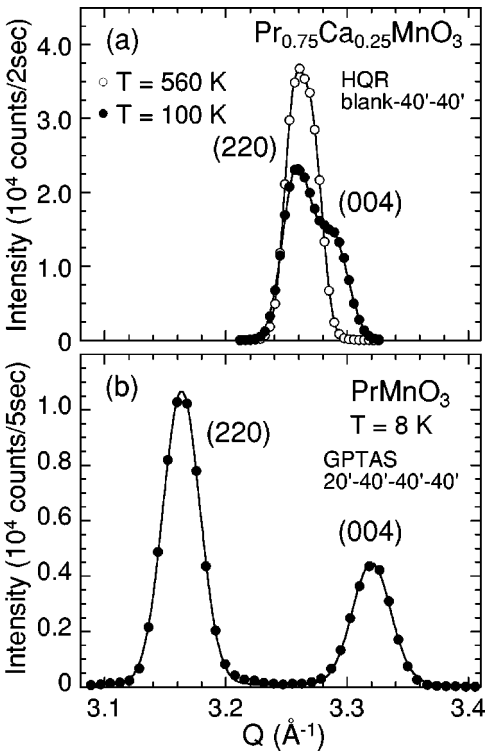

FIG. 4. Profiles of the 220/004 doublets along the [110] direction for (a) $Pr_{0.75}Ca_{0.25}MnO_3$ at 560 K and 100 K and (b) for $PrMnO_3$ at 8 K. The horizontal axes indicate the amplitudes of the scattering vector Q. Solid lines are fits to two Gaussians.

splitting of the two peaks in $Pr_{0.75}Ca_{0.25}MnO_3$ are much smaller than those observed in $PrMnO_3$.

Figure 5 shows typical profiles of constant-energy scans of spin wave excitations along the out-of-plane direction [001] (left panel) and the in-plane direction [110] (right panel) of $Pr_{0.75}Ca_{0.25}MnO_3$. The data were collected near the FM Bragg point (0,0,2) at $T=8$ K. The magnetic origin of these excitations were confirmed by measuring their Q dependence. The peak positions get away from the zone center as the energy increases according to the dispersion relation of the spin wave. From these measurements, we obtained the dispersion relation of the spin wave along the two directions, which is shown in Fig. 6. Note that the momentum transfer $\boldsymbol{q}=(0,0,2n)$ has almost the same magnitude as $\boldsymbol{q}=(n,n,0)$ in the *Pbnm* notation. In contrast to the $LaMnO_3$,[4,5] two dispersion curves well coincide, indicating that the spin exchange is isotropic ($J_{ab}\sim J_c$). This is consistent to the critical exponent β (Sec. III A), which is almost the same as the value for a 3D system. The observed dispersion curves can be described by the conventional FM Heisenberg model: $\mathcal{H}=-\Sigma_{ij}J_{ij}\boldsymbol{S}_i\cdot\boldsymbol{S}_j$, where J_{ij} is the exchange integral between spins at site $\boldsymbol{R}_i$ and $\boldsymbol{R}_j$. In the linear approximation, the dispersion relation is given by $\hbar\omega(\boldsymbol{q})=\Delta+2S[J(\boldsymbol{0})-J(\boldsymbol{q})]$, where $J(\boldsymbol{q})=\Sigma_j J_{ij}\exp[i\boldsymbol{q}\cdot(\boldsymbol{R}_i-\boldsymbol{R}_j)]$ and Δ accounts for small anisotropies. Taking only the isotropic nearest neighbor coupling J into account is sufficient to reproduce the observed data, and we get the solid line in Fig. 6 with $2JS=4.0(2)$ meV and $\Delta=0.0(3)$ meV.

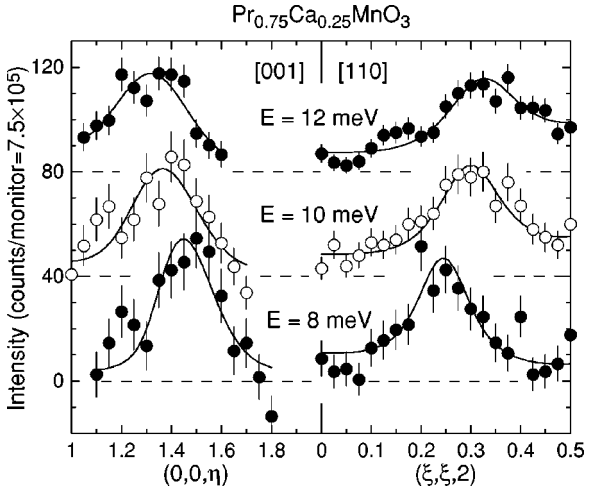

FIG. 5. Profiles of constant-energy scan of the magnon spectra along the [001] direction (left), and the [110] direction (right). The background is subtracted from each datum. The vertical axes are shifted by 40 counts for each energy. Solid lines are fits to the Lorentzian spectral function convoluted with the instrumental resolution.

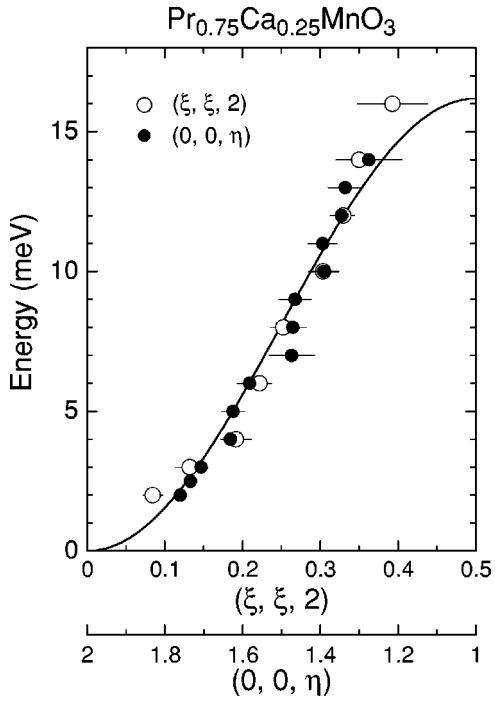

FIG. 6. Spin wave dispersion relations in $Pr_{0.75}Ca_{0.25}MnO_3$ along the [110] and [001] directions at 8 K. The solid line is a dispersion curve for the FM Heisenberg model with an isotropic nearest neighbor coupling.

The isotropic character of the spin system shows an interesting resemblance among the orbital-ordered FM-I phase and the orbital-disordered FM-M phase. However, one can distinguish them by the magnitude of the spin exchange. A clear enhancement of the spin stiffness $D(T)$ on the transition from the FM-I phase to the FM-M phase has been observed in a hole concentration dependence of $La_{1-x}Sr_xMnO_3$ (Ref. 30) and $La_{1-x}Ca_xMnO_3$ (Ref. 31) by neutron scattering

studies. The same phenomenon on the field-induced IM transition in $Pr_{0.7}Ca_{0.3}MnO_3$ has also been observed.[32] In these materials, $D(0)$ in the insulating phase is ≈ 50 meVÅ^2 and that in the metallic phase is ≈ 150 meVÅ^2. If we estimate $D(0)$ of the present $Pr_{0.75}Ca_{0.25}MnO_3$ compound from J at 8 K by a relation $D=2JSa_c^2$ where a_c is the lattice constant of the cubic lattice, $D(0)$ becomes ≈ 60 meVÅ^2. This value is almost same as that of the insulating $La_{1-x}Sr_xMnO_3$, $La_{1-x}Ca_xMnO_3$, and $Pr_{0.7}Ca_{0.3}MnO_3$. This fact evidences the common ground of the FM-I phase of the manganites.

The Jahn-Teller type lattice distortion means that there may exist a $LaMnO_3$-like OO as reported by the RXS study. Its smallness and the isotropy in J, however, suggest that the electron distribution is more isotropic than that in the $LaMnO_3$-type OO. A similar situation is realized in the FM-I phase of $La_{0.88}Sr_{0.12}MnO_3$,[20,33] where the staggered orbital ordering of $(|d_{3z^2-r^2}\rangle \pm |d_{x^2-y^2}\rangle)/\sqrt{2}$ is proposed.[20,21] In Sec. III C, we will theoretically investigate the orbital state $Pr_{1-x}Ca_xMnO_3$ and construct the spin and orbital phase diagrams.

C. Theory

Spin and orbital states in manganites with moderate hole doping are examined theoretically from the viewpoint of strong electron correlation. We adopt the t-J type Hamiltonian where the double degeneracy of the e_g orbitals is taken into account. The model Hamiltonian consists of the following four terms[34]:

$$\mathcal{H}=\mathcal{H}_t+\mathcal{H}_J+\mathcal{H}_H+\mathcal{H}_{AF}. \tag{1}$$

The first and second terms are the main terms corresponding to the t and J terms in the t-J model, respectively, given by

$$\mathcal{H}_t=\sum_{\langle ij\rangle\gamma\gamma'\sigma} t_{ij}^{\gamma\gamma'}\tilde{d}_{i\gamma\sigma}^{\dagger}\tilde{d}_{j\gamma'\sigma}+\text{H.c.} \tag{2}$$

and

$$\mathcal{H}_J=-2J_1\sum_{\langle ij\rangle}\left(\frac{3}{4}n_in_j+\vec{S}_i\cdot\vec{S}_j\right)\left(\frac{1}{4}n_in_j-\tau_i^l\tau_j^l\right) -2J_2\sum_{\langle ij\rangle}\left(\frac{1}{4}n_in_j-\vec{S}_i\cdot\vec{S}_j\right)\left(\frac{3}{4}n_in_j+\tau_i^l\tau_j^l+\tau_i^l+\tau_j^l\right). \tag{3}$$

$\tilde{d}_{i\gamma\sigma}$ is the annihilation operator of the e_g electron at site i with orbital γ and spin σ. This operator is defined in the restricted Hilbert space where the e_g electron numbers at each Mn site are limited to be one or less. The prefactor $t_{ij}^{\gamma\gamma'}$ is the transfer integral between orbital γ at sites i and γ' at j. $\mathcal{H}_J$ describes the superexchange interactions between the nearest neighboring Mn spins and orbitals. The spin and orbital degrees of freedom for the e_g electron are represented by the spin operator

$$\vec{S}_i=\frac{1}{2}\sum_{\gamma\sigma\sigma'}\tilde{d}_{i\gamma\sigma}^{\dagger}\vec{\sigma}_{\sigma\sigma'}\tilde{d}_{i\gamma\sigma'}, \tag{4}$$

and the pseudospin operator

$$\vec{T}_i=\frac{1}{2}\sum_{\gamma\gamma'\sigma}\tilde{d}_{i\gamma\sigma}^{\dagger}\vec{\sigma}_{\gamma\gamma'}\tilde{d}_{i\gamma'\sigma}, \tag{5}$$

respectively, with the Pauli matrices $\vec{\sigma}$. τ_i^l in $\mathcal{H}_J$ is defined by the pseudospin operator as

$$\tau_i^l=\cos\left(\frac{2m_l\pi}{3}\right)T_{iz}+\sin\left(\frac{2m_l\pi}{3}\right)T_{ix}, \tag{6}$$

with $(m_x,m_y,m_z)=(1,2,3)$ where $l(=x,y,z)$ indicates a direction of the bond connecting site i and site j. The magnitudes of the superexchange interactions J_1 and J_2 satisfy the condition $J_1>J_2>0$. The third and fourth terms in the Hamiltonian [Eq. (1)] describe the Hund coupling $J_H(>0)$ between the e_g and t_{2g} spins,

$$\mathcal{H}_H=-J_H\sum_i\vec{S}_i\cdot\vec{S}_{ti}, \tag{7}$$

and the AF superexchange interaction $J_{AF}(>0)$ between the nearest neighboring t_{2g} spins,

$$\mathcal{H}_{AF}=J_{AF}\sum_{\langle ij\rangle}\vec{S}_{ti}\cdot\vec{S}_{tj}, \tag{8}$$

respectively. $\vec{S}_{ti}$ is the spin operator for the t_{2g} electrons with $S=3/2$. It was confirmed that this model is successful in a description of the spin and orbital ordered states in hole doped and undoped manganites.[21,34]

Here, we examine the orbital ordered and disordered states in a unified fashion by applying the generalized slave boson method. The electron annihilation operator $\tilde{d}_{i\gamma\sigma}$ is decomposed into holon h_i, spinon $s_{i\sigma}$, and pseudospinon $t_{i\gamma}$ operators as

$$\tilde{d}_{i\gamma\sigma}=h_i^{\dagger}s_{i\sigma}t_{i\gamma}, \tag{9}$$

with local constraints of

$$h_i^{\dagger}h_i+\sum_{\gamma}t_{i\gamma}^{\dagger}t_{i\gamma}=1 \tag{10}$$

and

$$\sum_{\sigma}s_{i\sigma}^{\dagger}s_{i\sigma}=\sum_{\gamma}t_{i\gamma}^{\dagger}t_{i\gamma} \tag{11}$$

at each Mn site. We choose that both the holon and spinon are bosons, and the pseudo-spinon is a fermion.[36–38] This is because (1) in the ferromagnetic metallic phase, a hole carrier is recognized to be a fermion with orbital degree of freedom which is treated by $h_i^{\dagger}t_{i\gamma}$; and (2) the fermionic operator for the orbital degree of freedom $t_{i\gamma}$ is suitable for describing the orbitally disordered state. We adopt a mean field approximation where we take the bond order parameters for the orbital,

$$\sum_{\gamma\gamma'}\langle t_{ii+l}^{\gamma\gamma'}t_{i\gamma}^{\dagger}t_{i+l\gamma'}\rangle=t_0\chi_t^l, \tag{12}$$

and those for the spin,

$$\sum_{\sigma} \langle s^{\dagger}_{i\sigma} s_{i+l\sigma} \rangle = \chi^{l}_{s}, \tag{13}$$

and the site diagonal order parameters for the orbital,

$$\sum_{\gamma\gamma'} \langle t^{\dagger}_{i\gamma} \sigma^{\mu}_{\gamma\gamma'} t_{i\gamma} \rangle = m^{\mu}_{t}(i), \tag{14}$$

for $\mu = x$ and z, and those for the spin,

$$\sum_{\sigma} \langle s^{\dagger}_{i\sigma} \sigma^{z}_{\sigma\sigma} s_{i\sigma} \rangle = m^{z}_{s}(i). \tag{15}$$

t_0 in Eq. (12) is the electron transfer intensity between the nearest neighboring $d_{3z^2-r^2}$ orbitals along the z axis. We also introduce a mean field for the holon,

$$\langle h^{\dagger}_{i} h_i \rangle = -\langle h^{\dagger}_{i} h_j \rangle = x, \tag{16}$$

with the hole concentration x. In this scheme, the local constraints are released into the global ones:

$$\sum_{i} \left(h^{\dagger}_{i} h_i + \sum_{\gamma} t^{\dagger}_{i\gamma} t_{i\gamma} \right) = 1 \tag{17}$$

and

$$\sum_{i\sigma} s^{\dagger}_{i\sigma} s_{i\sigma} = \sum_{i\gamma} t^{\dagger}_{i\gamma} t_{i\gamma}. \tag{18}$$

By considering the strong Hund coupling J_H, the directions of $\vec{S}_i$ and $\vec{S}_{ti}$ are assumed to be the same. The effects of the lattice distortion and its coupling to the e_g electrons are not considered explicitly in the present model. This is because, in the moderately hole doped region of our interest, the Jahn-Teller distortion is significantly reduced as shown in Sec. III B.

The phase diagram is obtained numerically by minimizing the free energy with respect to the order parameters (Fig. 7). The parameter values are chosen to be $J_2/J_1 = 0.25$, $J_{AF}/J_1 = 0.014$, and $t_0/J_1 = 2$. For the Fourier transform of the site diagonal order parameters $m^{\mu}_{t}(\vec{k})$ and $m^{z}_{s}(\vec{k})$, we assume that $m^{x}_{t}(\pi\pi 0)$, $m^{z}_{t}(000)$, $m^{z}_{s}(00\pi)$ and $m^{z}_{s}(000)$ are finite in the ordered phases. Below the orbital ordering temperature T_{OO}, the site diagonal orbital order parameters $m^{\mu}_{t}(\vec{k})$ appear. T_C and T_N are the Curie temperature and the Néel temperature for the A-type AF order, where $m^{z}_{s}(000)$ and $m^{z}_{s}(00\pi)$ appear, respectively. At $x = 0$, the staggered type orbital order $m^{x}_{t}(\pi\pi 0)$ occurs far above T_N, as observed in $LaMnO_3$ and $PrMnO_3$. By taking into account the cooperative Jahn-Teller effects which is not included in the present calculation, T_{OO} may increase from the calculated value. With a doping of the holes, T_{OO} rapidly decreases and disappears around $x = 0.15 (\equiv x_c)$. Above x_c, $m^{\mu}_{t}(\vec{k})$ becomes zero, but the bond order parameters $\chi^{l}_{t}(\vec{k})$ still remain finite. That is, the orbital liquid state is realized above the critical point x_c. As for the magnetic ordering, the A-type AF phase is changed into the FM phase through the canted AF

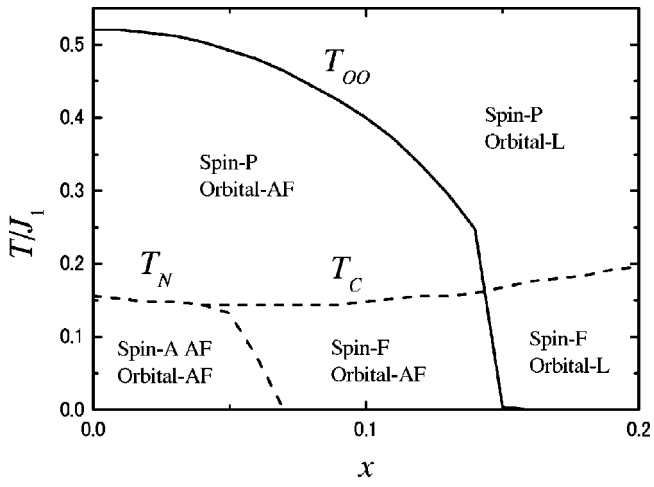

FIG. 7. The spin and orbital phase diagram in the hole concentration x and temperature T plane. The parameter values are chosen to be $J_2/J_1 = 0.25$, $J_{AF}/J_1 = 0.014$, and $t_0/J_1 = 2$. F, AF, P, and L indicate the ferromagnetic phase, the antiferromagnetic phase, the paramagnetic phase, and the orbital liquid phase, respectively.

one, which is observed in $Pr_{1-x}A_xMnO_3$.[39] The x dependence of T_C/T_N is almost flat below $x = 0.1$ and slightly increases with increasing x. The ground state electronic phases are classified into (I) the (canted) A-type AF phase with the staggered OO corresponding to $LaMnO_3$ and $PrMnO_3$, (II) the FM phase with the staggered OO which is discussed later in more detail, and (III) the FM phase with the orbital liquid state corresponding to the FM-M state in heavily hole doped manganites, such as $La_{1-x}Sr_xMnO_3$ with $x \sim 0.3$. In a series of $Pr_{1-x}Ca_xMnO_3$, it is interpreted that this phase does not appear because the charge ordered AF insulating phase is stable down to the region of $x \sim 0.3$ instead of this FM-M phase.

Now we focus on the FM phase with the staggered OO. We interpret that this corresponds to the FM phase in $Pr_{1-x}Ca_xMnO_3$ with $0.15 < x < 0.3$ of our present interest. The OO in this FM phase is of the staggered type, where the two kinds of orbital are characterized by the orbital mixing angles $(\theta/-\theta)$, as well as the OO in the A-type AF phase. This angle is defined as $|\theta\rangle = \cos(\theta/2)|d_{3z^2-r^2}\rangle + \sin(\theta/2)|d_{x^2-y^2}\rangle$. This is consistent with the azimuthal angle scan of the RXS experiments in $Pr_{0.75}Ca_{0.25}MnO_3$; the azimuthal angle φ is the rotation angle of the sample around the x-ray scattering vector $\vec{k}_i - \vec{k}_f$ in the RXS experiments. By measuring the φ dependence of the RXS intensity $I(\varphi)$, the information for the symmetry of the orbital ordered states is deduced.[35] The experimentally observed $I(\varphi)$ in $Pr_{0.75}Ca_{0.25}MnO_3$ is proportional to a function $\sin^2\varphi$ which is consistent with the theoretical prediction for $I(\varphi)$ in the OO state of the $(\theta/-\theta)$ type.[22,35] The value of θ in the present calculation is about π. That is, the orbital wave functions are given by $(|d_{3z^2-r^2}\rangle \pm |d_{x^2-y^2}\rangle)/\sqrt{2}$ where the electronic clouds are more elongated along the z direction in comparison with the $d_{3x^2-r^2}$ and $d_{3y^2-r^2}$ orbitals. It is noted that, with doping of holes, the saturated orbital moment $|m^{\mu}_{t}|$ gradually decreases, and finally disappears at x_c. On the

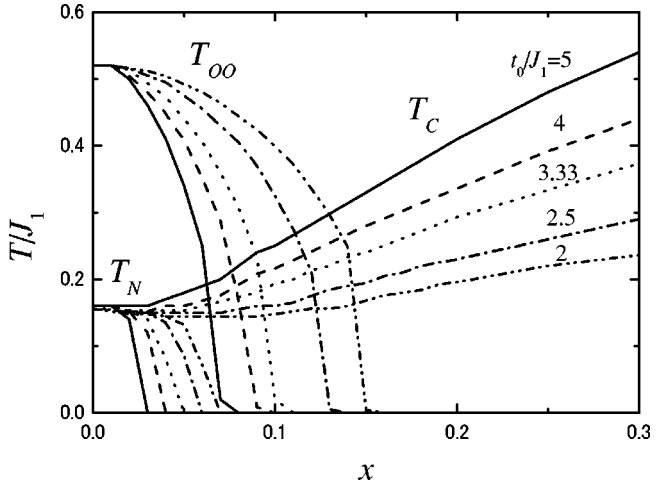

FIG. 8. The spin and orbital phase diagram as functions of t_0/J_1. The parameter values are chosen to be $J_2/J_1=0.25$ and $J_{AF}/J_1=0.014$.

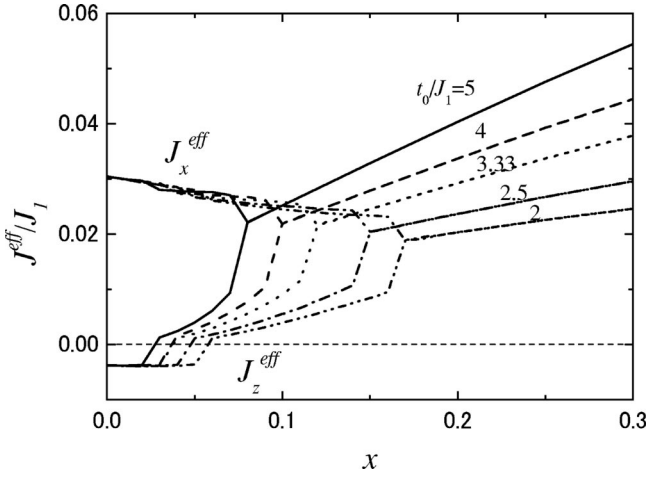

FIG. 9. The x dependence of the effective exchange interaction J_x^{eff} and J_z^{eff}. The parameter values are chosen to be $J_2/J_1=0.25$ and $J_{AF}/J_1=0.014$.

other hand, the bond variable $|\chi_t^l|$ grows from zero at $x=0$. That is, the two FM interactions, i.e., the double exchange interaction based on the kinetic term $\mathcal{H}_t$ and the superexchange FM one from $\mathcal{H}_J$, coexist. This is consistent with the present experimental results in $Pr_{0.75}Ca_{0.25}MnO_3$ that the magnitude of the Jahn-Teller distortion, related to the magnitude of the diagonal order parameters m_t^μ, is significantly reduced in comparison with that in $PrMnO_3$. Unfortunately, in this calculation, this FM phase is not insulating, because the translational symmetry is assumed in the mean field approximation. However, we numerically confirm that the band width of the charge carriers, which is proportional to the bond order parameter χ_t^l, is much reduced in the orbital ordered FM phase in comparison with that in the FM orbital liquid phase. We believe that doped carriers in such a narrow band tend to be localized by other ingredients which are not taken into account in the present model.

We also examine the phase diagram by changing the relative ratio of the kinetic energy and the exchange energy $t_0/J_{1(2)}$ (Fig. 8). With decreasing $t_0/J_{1(2)}$, the critical hole concentration x_c, where T_{OO} disappears, increases, and the region of the orbital ordered FM phase is extended to the region with higher x. On the other hand, T_C in the FM-M phase is reduced, and T_N and T_C become less sensitive to x. These calculated results may explain a difference of the phase diagrams of $La_{1-x}Sr_xMnO_3$ (LSMO), $La_{1-x}Ca_xMnO_3$ (LCMO), and $Pr_{1-x}Ca_xMnO_3$ (PCMO). The parameter value of $t_0/J_{1(2)}$ in the calculation is expected to decrease in this order of the materials. The FM-I phase is realized in the regions of $0.1<x<0.15$ for LSMO, $0.12<x<0.22$ for LCMO, and $0.15<x<0.3$ for PCMO; the FM-I phase is extended and shifts to the region with higher x. T_C in the FM-M phase in LSMO is almost twice of T_N in $LaMnO_3$. On the other hand, difference between T_N in $PrMnO_3$ and T_C in PCMO with $x=0.3$ is about 30% of the T_N.

In order to examine the spin dynamics in the orbital ordered FM phase, we calculate the spin stiffness by applying the linear spin wave theory to the model Hamiltonian in Eq. (1). The effective exchange interaction J^{eff} corresponding to the interaction J_l along the direction $l(=x,y,z)$ in the Heisenberg model, $-\Sigma_{\langle ij\rangle}J_l^{eff}\vec{S}_i\cdot\vec{S}_j$ is obtained as

$$J_l^{eff}=\frac{-D_l^t+2D_l^J}{2S^2}. \tag{19}$$

D_l^t is the stiffness constant arising from the transfer term of the Hamiltonian $\mathcal{H}_t$ given by

$$D_l^t=xt_0\chi_t^l, \tag{20}$$

and D_l^J is the one from $\mathcal{H}_J$ and $\mathcal{H}_{AF}$ given by

$$D_l^J=-J_l\frac{1}{4}-J_{AF}\frac{9}{4}, \tag{21}$$

with

$$J_x=-\frac{1}{2}(J_1-3J_2)(1-x)^2 + \frac{1}{2}(J_1+J_2)\left(\frac{1}{4}m_t^{z2}-\frac{3}{4}m_t^{x2}-4\chi_t^{x2}\right)-J_2m_t^z, \tag{22}$$

and

$$J_z=-\frac{1}{2}(J_1-3J_2)(1-x)^2 + \frac{1}{2}(J_1+J_2)\left(\frac{1}{2}m_t^{z2}-4\chi_t^{z2}\right)+2J_2m_t^z. \tag{23}$$

Here, we define the average magnitude of the Mn spin as $S=(1-x)/2+3/2$. The x dependence of the effective exchange interactions, $J_x(=J_y)$ and J_z, are presented in Fig. 9. In the A-type AF phase near $x=0$, J_z is negative and its magnitude is much weaker than that of $|J_x|$. This is experimentally confirmed by the inelastic neutron scattering in

$LaMnO_3$. With a doping of the holes, the sign of J_z is changed to a positive one, and J_x decreases and J_z increases. That is, the anisotropy of the exchange interactions is much reduced. This tendency of the x dependence of the anisotropy of J_l^{eff} is consistent with the present neutron-scattering experiments in $Pr_{1-x}Ca_xMnO_3$, although, in the calculation, the weak anisotropy of J^{eff} remains in the orbital ordered FM phase. Such an anisotropy may not be detected due to the coarse resolution of the present neutron scattering experiments.

IV. CONCLUSION

We have systematically investigated the nature of the FM-I state of perovskite manganites by a neutron scattering study on a single crystal of $Pr_{0.75}Ca_{0.25}MnO_3$ and theoretical calculations. We have found that (1) the insulating behavior is robust against an external magnetic field, (2) the FM moment is almost fully polarized, (3) the Jahn-Teller lattice distortions are strongly suppressed, and (4) the spin exchange interactions are isotropic. These features are against interpretations of insulating behavior based on COs or phase separation, and are consistent to the staggered type orbital ordered state. The spin stiffness is similar to those observed in other FM-I manganites and has a smaller value than that in the FM-M phase, indicating the ubiquitous origin of the FM-I state. We theoretically construct the comprehensive spin and orbital phase diagram for the FM phase, which can explain the difference of the phase diagrams of several manganites.

Finally, we should note the importance of our work for the research of the IM transition or the CMR phenomenon in hole-doped perovskite manganites. Many previous experimental researches focusing attention on the phase separation as an origin of the IM transition attribute an isotropic phase or a FM phase to a metallic phase. However, the existence of an *isotropic ferromagnetic* insulating phase means one must pay better attention to identifying the metallic phase and consider the effect of the staggered type OO especially in the low-doped region.

ACKNOWLEDGMENTS

This work was supported by KAKENHI from MEXT. Part of the numerical calculation was performed in the superconducting facilities in the Institute for Materials Research, Tohoku University. R.K. was supported by the Japan Society for the Promotion of Science.

*Present address: Neutron Science Laboratory, Institute of Materials Structure Science, High Energy Accelerator Research Organization, 1-1 Oho, Tsukuba, Ibaraki 305-0801, Japan. Electronic address: kaji@post.kek.jp.

†Present address: Department of Physics, Columbia University, 538 West 120th Street, New York, 10027, USA.

[1] J. Rodriguez-Carvajal, M. Hennion, F. Moussa, A.H. Moudden, L. Pinsard, and A. Revcolevschi, Phys. Rev. B **57**, R3189 (1998).

[2] Y. Murakami, J.P. Hill, D. Gibbs, M. Blume, I. Koyama, M. Tanaka, H. Kawata, T. Arima, Y. Tokura, K. Hirota, and Y. Endoh, Phys. Rev. Lett. **81**, 582 (1998).

[3] M. Imada, A. Fujimori, and Y. Tokura, Rev. Mod. Phys. **70**, 1039 (1998).

[4] K. Hirota, N. Kaneko, A. Nishizawa, and Y. Endoh, J. Phys. Soc. Jpn. **65**, 3736 (1996).

[5] F. Moussa, M. Hennion, J. Rodríguez-Carvajal, H. Moudden, L. Pinsard, and A. Revcolevschi, Phys. Rev. B **54**, 15149 (1996).

[6] P.G. de Gennes, Phys. Rev. **118**, 141 (1960).

[7] S. Ishihara, M. Yamanaka, and N. Nagaosa, Phys. Rev. B **56**, 686 (1997).

[8] A. Urushibara, Y. Moritomo, T. Arima, A. Asamitsu, G. Kido, and Y. Tokura, Phys. Rev. B **51**, 14103 (1995).

[9] Michael C. Martin, G. Shirane, Y. Endoh, K. Hirota, Y. Moritomo, and Y. Tokura, Phys. Rev. B **53**, 14285 (1996).

[10] T.G. Perring, G. Aeppli, S.M. Hayden, S.A. Carter, J.P. Remeika, and S.-W. Cheong, Phys. Rev. Lett. **77**, 711 (1996).

[11] Y. Tomioka, A. Asamitsu, H. Kuwahara, Y. Moritomo, and Y. Tokura, Phys. Rev. B **53**, R1689 (1996).

[12] H. Yoshizawa, H. Kawano, Y. Tomioka, and Y. Tokura, Phys. Rev. B **52**, R13145 (1995).

[13] H. Yoshizawa, H. Kawano, Y. Tomioka, and Y. Tokura, J. Phys. Soc. Jpn. **65**, 1043 (1996).

[14] Pengcheng Dai, J.A. Fernandez-Baca, N. Wakabayashi, E.W. Plummer, Y. Tomioka, and Y. Tokura, Phys. Rev. Lett. **85**, 2553 (2000).

[15] M. Uehara, S. Mori, C.H. Chen, and S.-W. Cheong, Nature (London) **399**, 560 (1999).

[16] D.E. Cox, P.G. Radaelli, M. Marezio, and S-W. Cheong, Phys. Rev. B **57**, 3305 (1998).

[17] T. Hotta and E. Dagotto, Phys. Rev. B **61**, R11879 (2000).

[18] T. Mizokawa, D.I. Khomskii, and G.A. Sawatzky, Phys. Rev. B **61**, R3776 (2000).

[19] T. Mizokawa, D.I. Khomskii, and G.A. Sawatzky, Phys. Rev. B **63**, 024403 (2000).

[20] Y. Endoh, K. Hirota, S. Ishihara, S. Okamoto, Y. Murakami, A. Nishizawa, T. Fukuda, H. Kimura, H. Nojiri, K. Kaneko, and S. Maekawa, Phys. Rev. Lett. **82**, 4328 (1999).

[21] S. Okamoto, S. Ishihara, and S. Maekawa, Phys. Rev. B **61**, 14647 (2000).

[22] M.v. Zimmermann, C.S. Nelson, J.P. Hill, Doon Gibbs, M. Blume, D. Casa, B. Keimer, Y. Murakami, C.-C. Kao, C. Venkataraman, T. Gog, Y. Tomioka, and Y. Tokura, Phys. Rev. B **64**, 195133 (2001).

[23] L. Vasiliu-Doloc, J.W. Lynn, Y.M. Mukovskii, A.A. Arsenov, and D.A. Shulyatev, J. Appl. Phys. **83**, 7342 (1998).

[24] Joonghoe Dho, E.O. Chi, N.H. Hur, K.W. Lee, H.S. Oh, and Y.N. Choi, Solid State Commun. **123**, 441 (2002).

[25] Strictly speaking, this position is where the superlattice peak due to the *CE*-type OO is expected. Because it has been confirmed that the OO and CO are intimately related in the *CE*-type CO (Ref. 26), we refer the *CE*-type OO peaks as *CE*-type CO peaks in the present paper.

[26] M.v. Zimmermann, J.P. Hill, Doon Gibbs, M. Blume, D. Casa, B. Keimer, Y. Murakami, Y. Tomioka, and Y. Tokura, Phys. Rev. Lett. **83**, 4872 (1999).

[27] S. Shimomura, N. Wakabayashi, H. Kuwahara, and Y. Tokura, Phys. Rev. Lett. **83**, 4389 (1999).
[28] C.P. Adams, J.W. Lynn, Y.M. Mukovskii, A.A. Arsenov, and D.A. Shulyatev, Phys. Rev. Lett. **85**, 3954 (2000).
[29] Z. Jirák, S. Krupička, Z. Šimša, M. Dlouhá, and S. Vratislav, J. Magn. Magn. Mater. **53**, 153 (1985).
[30] Y. Endoh and K. Hirota, J. Phys. Soc. Jpn. **66**, 2264 (1997).
[31] Pengcheng Dai, J.A. Fernandez-Baca, E.W. Plummer, Y. Tomioka, and Y. Tokura, Phys. Rev. B **64**, 224429 (2001).
[32] J.A. Fernandez-Baca, Pengcheng Dai, H. Kawano-Furukawa, H. Yoshizawa, E.W. Plummer, S. Katano, Y. Tomioka, and Y. Tokura, Phys. Rev. B **66**, 054434 (2002).
[33] K. Hirota, N. Kaneko, A. Nishizawa, Y. Endoh, M.C. Martin, and G. Shirane, Physica B **237-238**, 36 (1997).
[34] S. Ishihara, J. Inoue, and S. Maekawa, Phys. Rev. B **55**, 8280 (1997).
[35] S. Ishihara and S. Maekawa, Phys. Rev. B **58**, 13442 (1998).
[36] G. Khaliullin and R. Kilian, Phys. Rev. B **61**, 3494 (2000).
[37] A.M. Oleś and L.F. Feiner, Phys. Rev. B **65**, 052414 (2002).
[38] K. Hirota, S. Ishihara, H. Fujioka, M. Kubota, H. Yoshizawa, Y. Moritomo, Y. Endoh, and S. Maekawa, Phys. Rev. B **65**, 064414 (2002).
[39] Z. Jirák, J. Hejtmánek, E. Pollert, M. Maryško, M. Dlouhá, and S. Vratislav, J. Appl. Phys. **81**, 5790 (1997).